Available online at www.sciencedirect.com

ScienceDirect

Scripta Materialia 100 (2015) 86–89

Scripta MATERIALIA

www.elsevier.com/locate/scriptamat

Terrace-like morphology of the boundary created through basal-prismatic transformation in magnesium

Bo-Yu Liu,[a] Liang Wan,[a] Jian Wang,[b] Evan Ma[a,c] and Zhi-Wei Shan[a,*]

[a]*Center for Advancing Materials Performance from the Nanoscale (CAMP-Nano) & Hysitron Applied Research Center in China (HARCC), State Key Laboratory for Mechanical Behavior of Materials, Xi'an Jiaotong University, Xi'an 710049, PR China*

[b]*MST-8, Los Alamos National Laboratory, Los Alamos, NM 87545, USA*

[c]*Department of Materials Science and Engineering, Johns Hopkins University, Baltimore, MD 21218, USA*

Received 19 November 2014; revised 28 December 2014; accepted 30 December 2014
Available online 24 January 2015

Boundaries created through basal-prismatic transformation in submicron-sized single crystal magnesium have been investigated systematically using in situ transmission electron microscopy. We found that these boundaries not only deviated significantly from the twin plane associated with $\{10\bar{1}2\}$ twin, but also possessed a non-planar morphology. After the sample was thinned to be less than 90 nm, aberration-corrected scanning transmission electron microscopy observation found that the basic components of these boundaries are actually terrace-like basal-prismatic interfaces.

Keywords: Basal-prismatic interface; Grain boundaries; Magnesium; TEM

At room temperature, dislocation slip [1] and deformation twinning [2,3] are known to be the main mechanisms of plastic deformation for crystalline metals. In these displacive processes, once lattice gliding dislocations (or twinning dislocations) run across the material, steps will be generated on the free surfaces with the magnitude being multiples of Burgers vector of the dislocation [4,5]. For magnesium having the hexagonal close packed (hcp) structure, it has been well accepted that $\{10\bar{1}2\}$ deformation twinning will be a major contributor to the plasticity [6,7], when the crystal is subjected to an effective tensile stress along the [0001] direction. Recently, we demonstrated that when submicron sized single crystal magnesium is deformed under compression along the $[1\bar{1}00]$ orientation or tension along the [0001] orientation, plastic strains can be accommodated by basal-prismatic (BP) transformation [8] which results in the effective reorientation of the hcp unit cell by about 90° around the $[11\bar{2}0]$ direction (*a*-axis). In this paper, for the sake of simplicity, we term this novel deformation mechanism as unit cell reconstruction (UCR).

Compared with deformation twinning, UCR in magnesium has several distinct features. First of all, it is the BP transformation at the BP interface that dominates the boundary migration instead of the gliding of twinning dislocations on twinning planes. Second, the boundary that separates the reoriented crystal from its parent crystal is not a crystallographic mirror plane. Third, UCR produces tetragonal deformation instead of simple shear [9,10]. These new features suggest that the boundary generated through UCR must be different from the boundaries produced by deformation twinning (twin boundaries). However, information regarding the morphology of such boundaries remains very limited [11–13]. In this work, we focus on the atomic-scale configurations of the boundaries generated through UCR, while their effects on the mechanical response will be discussed in future.

Submicron-sized single-crystal magnesium samples used in this work were fabricated with exactly the same method reported in our previous work, employing focused ion beam (FIB, Helios 600, FEI) micromachining [8]. Figure 1 shows the typical SEM images of a pillar sample (Fig. 1a) and a dog-bone shaped sample (Fig. 1b). Compression tests were conducted both on pillar samples and dog-bone samples. Tension tests were applied on dog-bone samples only. The axial direction of the compressive samples was designed to be $[1\bar{1}00]$ and that for tensile samples was [0001]. The viewing direction for pillar samples was designed to be $[11\bar{2}0]$ or [0001], and for dog-bone samples it was $[11\bar{2}0]$. The cross-section of these samples was close to square shape. The nominal sample size, defined as the square root of the cross-sectional area of the samples, ranged from 100 nm to 500 nm. The aspect ratio of the pillar samples ranged from 3:1 to 4:1, and that of dog-bone samples ranged from 4:1 to 10:1. In tension tests, the entire gauge volume tends to be converted into the new grain

* Corresponding author. Tel.: +86 29 82668824; e-mail: zwshan@mail.xjtu.edu.cn

http://dx.doi.org/10.1016/j.scriptamat.2014.12.020
1359-6462/

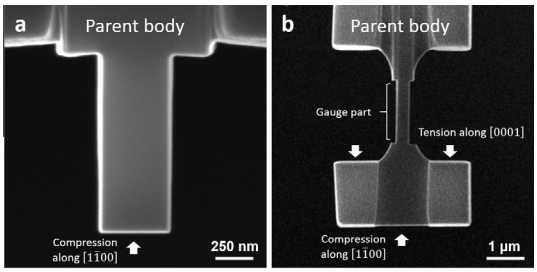

Figure 1. SEM images showing the typical sample geometry and loading conditions. (a) A pillar sample. (b) A dog-bone sample. In compression tests the external load was applied to the bottom surface via a diamond probe. In tension tests the pulling force was applied to the two shoulders (indicated by the two white arrows) by a specially designed diamond gripper.

within a single strain burst when the aspect ratio is small [8]. Therefore, longer dog-bone samples allowed us to monitor the boundary migration process within the gauge part during tensile loading. All the mechanical tests reported in this paper were carried out using Hysitron PI95 Picoindenter under displacement control mode inside a transmission electron microscope (TEM, JEOL 2100F, 200 keV) [14]. The probe velocity was set to be 5 nm/s which corresponded to a strain rate in the order of 10^{-3}/s.

In order to reveal the 3D morphology of the boundaries created by UCR, we not only examined the sample from two orientations, but also purposely thinned a typical sample using FIB from 500 nm down to 90 nm. This sectioning allowed us to investigate the change of the projected boundary profile. However, FIB machining will introduce surface damage layer with a thickness of tens of nanometers, which makes it difficult to thin a 90 nm sample. We therefore employed a Nano Mill (M1040, Fischione) for the final thinning process, where the damaged layer can be as thin as 2 nm. After that, an ARM200F spherical aberration-corrected TEM (200 keV) was used under the scanning TEM (STEM) mode, which avoids the delocalization effects in imaging.

Regardless of compression or tension, a new grain always forms in our single crystal magnesium samples, creating a boundary between the new grain and the matrix. Selected area diffraction analysis found that for all the samples reported in this work, the basal plane of the new grain and that of the matrix is always perpendicular to each other. Given the observation direction along [1 1 $\bar{2}$ 0], if we define the angle between the trace line of the boundary and the loading direction as α, then the α expected for $\{10\bar{1}2\}$ deformation twinning will be 43.15° for compression and 46.85° for tension. However, measurements for 16 boundaries indicate that the α is statistically inconsistent with that expected from $\{10\bar{1}2\}$ deformation twinning (Fig. 2a). This conclusion is supported by the morphology of the newly formed boundaries: some of them are even parallel with or perpendicular to the loading direction, and some of them exhibit considerable width. Typical examples corresponding to these three scenarios are shown in Figure 2b–d.

Figure 2b is a typical example showing a newly formed boundary parallel to the loading axis. The postmortem TEM dark field image was taken at the root part of this sample. The new grain was formed during a strain burst. As shown in Figure 2b, one of its ends penetrated into

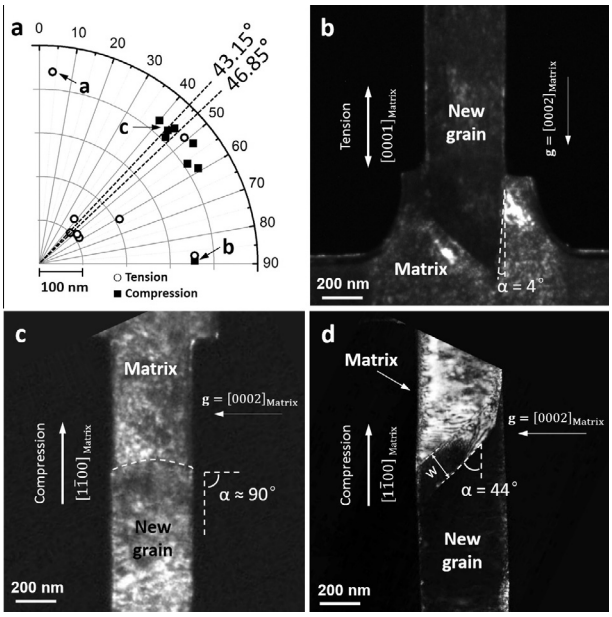

Figure 2. Statistic measurement of the angle α between the trace line of the boundary and the loading direction. (a) A protractor diagram shows the distribution of the angle α measured from 16 boundaries. The radial axis represents the diameter of samples. The theoretical angle α for $\{10\bar{1}2\}$ twinning are marked using dashed lines. (b), (c) and (d) are dark field TEM images that correspond to the angle α marked in (a) respectively.

the matrix like a dagger, instead of stopping at the end of the gauge part, with a boundary almost aligned with the extrapolation of the right surface of the gauge part, as delineated by the dashed white lines. Another extreme case is shown in Figure 2c. This image was a snapshot extracted from a movie recorded during the compression test of a pillar sample. The migrating boundary appeared to be in an arched shape and almost perpendicular to the loading direction, as outlined by the white dashed line in Figure 2c. In addition, for the given viewing direction, the sample was observed to widen toward both sides symmetrically along with the propagation of the boundary and no simple shear was observed. Conventional plastic deformation mechanisms, either an ordinary dislocation slip or deformation twining, appear to be inadequate to explain these phenomena [8].

Besides the two extreme cases described above, another very interesting feature of the boundaries created by UCR is that they may exhibit considerable width when viewed along [1 1 $\bar{2}$ 0]. This is unexpected because both the twin plane and the BP interface should appear edge on for the given observation direction. One typical example is shown in Figure 2d. This pillar sample has a nominal size of 424 nm. Even though the $\alpha = 44°$ is close to the theoretical value for $\{10\bar{1}2\}$ deformation twinning, two nearly parallel trace lines instead of one can be seen clearly in between the new grain and its matrix, with the width (w) of about 120 nm. In addition, the contrast in the area framed by these two trace lines is not uniform, with its left lower part close to that of the new grain (dark) and its upper right part close to that of the matrix (bright). On the one hand, it indicates that the volume fraction of the new grain along the thickness direction is not uniform inside the band; on the other hand, it simply rules out the possibility that the band

like boundary is due to a deviation from the designed imaging direction. Examination of the corresponding movie recorded during the compression test found that the new grain expanded through the migration of such a band-like boundary, but the two trace lines did not move synchronously. The front trace line moved earlier than the back one, and interestingly, it retreated for tens of nanometers during the unloading process.

To reveal the origin of this band-like feature of the boundary in 3D, we monitored the boundary migration process in another pillar compression test under the same loading condition but with the viewing direction of [0001], which is perpendicular to the former viewing direction $[11\bar{2}0]$ used in Figure 2. Figure 3 presents four snapshots captured from the movie recorded in this test. Figure 3a shows the newly formed grain (dark contrast) that just nucleated within a strain burst. Under the given viewing axis, this new grain exhibited a wedge shape with its upper boundary line not parallel to its bottom boundary line. Obviously, the boundary was not parallel to the $[11\bar{2}0]$ direction, which led to the projected area when viewed along $[11\bar{2}0]$ in Figure 2d. The most front and back parts of the boundary were projected to be the front and back trace lines of the band-like area. The intercept distance along the $[1\bar{1}00]_{Matrix}$ orientation of this boundary was about 180 nm, which was comparable to the width shown in Figure 2d. The boundary then migrated upward under the compressive loading, as shown in Figure 3b. Note that the intercept distance increased to about 280 nm, which means part of the boundary moved faster. It coincides with the unsynchronized migration of the two boundary trace lines in the previous observation (Fig. 2d). Very interestingly, the boundary bowed into a convex shape during its migration. This demonstrates that the boundary created through UCR was not confined to a single crystallographic plane. This highly incoherent boundary is in sharp contrast to $\{10\bar{1}2\}$ twin boundaries created by deformation twinning. Figure 3c shows the peak volume of the new grain just before unloading and Figure 3d shows that the new grain shrank after the diamond probe was retracted completely. Correspondingly, the intercept distance decreased from 230 nm to about 180 nm, which also coincided with the retreat of the front trace line during unloading in the previous observation (Fig. 2d). This indicates that part of the new grain could be converted back to its matrix during the unloading process even before the compressive stress dropped to zero.

The above examination demonstrated that the band-like feature was actually the projected area of a 3D curved boundary. Therefore, such a projected area should become narrower when the sample thickness is reduced and the BP interfaces will finally emerge if the sample is thin enough. We chose one deformed pillar sample with a band-like boundary and thinned it several times to different thicknesses purposely to investigate if the projection width is related to the sample thickness. Results are shown in Figure 4. Dark field TEM image of part of the as-deformed pillar is shown in Figure 4a. Similar to that shown in Figure 2d, the contrast of the band-like boundary exhibits a gradient along the trace line direction. Figure 4b is the magnified image of the area framed by the white dashed box in Figure 4a. At this point, the sample thickness (t) was about 500 nm, and the width (w) of the projected boundary area was about 145 nm. The width decreased to about 65 nm

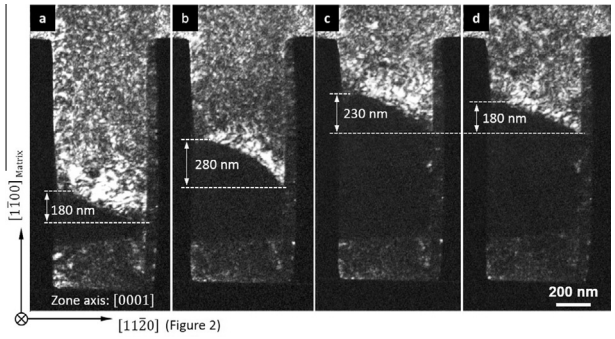

Figure 3. TEM snapshots showing the evolution of a migrating boundary viewed from [0001]. (a) The new grain (dark contrast) just nucleated. (b) The new grain is expanding with an arch shaped boundary. (c) The pillar was under the largest strain. (d) The probe was completely retracted.

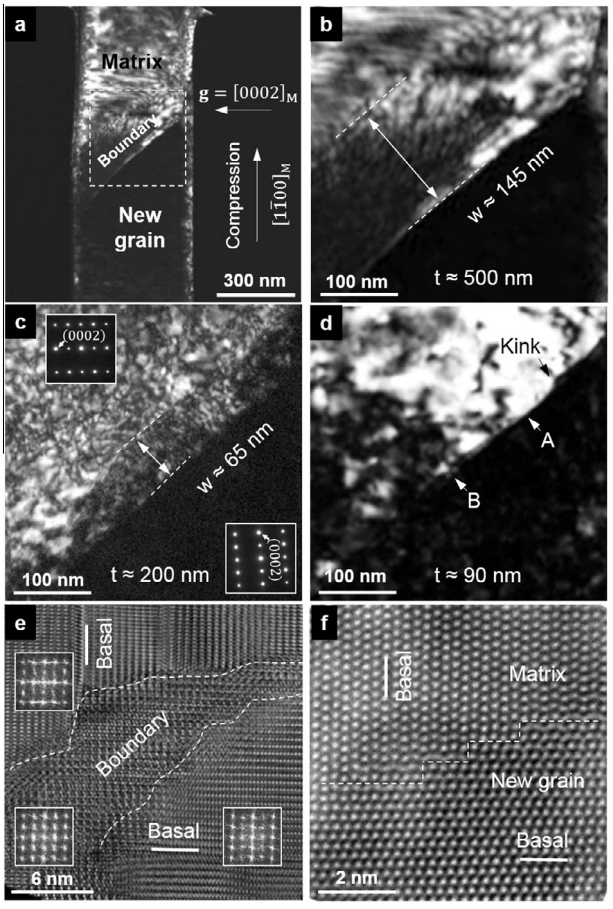

Figure 4. Morphologies of the projected boundary with respect to the reduced sample thickness. (a) Dark field TEM image of a deformed pillar. (b), (c) and (d) are images taken in the white framed region in (a) when the sample was thinned to 500 nm, 200 nm and 90 nm, respectively. The zone axis is $[11\bar{2}0]$. Insets in (c) are selected area diffraction patterns acquired from the matrix and the new grain respectively. (e) HRTEM image acquired from the boundary area in (d). The boundary profile is outlined using dashed lines. Insets are fast Fourier transform images taken from the matrix, the new grain and the boundary, respectively. (f) Atomic structure of BP interfaces when the sample thickness is reduced below 90 nm. The BP interfaces are outlined by dashed lines.

when the sample was thinned to about 200 nm, as shown in Figure 4c. It was interesting to note that the contrast distribution inside the band is different from that shown in Figure 4b. If we assume that the gray level of the contrast is proportional to the volume fraction of the matrix in the sample thickness direction, it again indicates the non-planar nature of the boundary. When the sample was further thinned to about 90 nm, parts of the boundary appeared to be a line, e.g. the area indicated by the white arrow A in Figure 4d, while other parts still appeared to be a band but became much narrower, e.g. the area indicated by the white arrow B. Note that the boundary was not straight but exhibited a wavy morphology and even contained some kinks, as indicated by the short black arrow. Although the boundary appears as a line at the current magnification shown in Figure 4d, high resolution TEM (HRTEM) demonstrated clearly its wavy and band-like feature on atomic scale. One typical example is shown in Figure 4e. The profile of the boundary area possessed an irregular shape, as outlined by the white dashed line. Fast Fourier transform images taken from different areas showed that the blurred boundary area is actually the overlap of the matrix and the new grain. After a final thinning process by Nano Mill, edge-on BP interfaces connecting the two grains were clearly revealed by Cs-corrected STEM imaging. The basal planes of the new grain and its matrix are highlighted with the solid white lines to demonstrate the orientation relationship.

As shown in Figure 4f, there are steps on the BP boundary and they are perpendicular to each other. Therefore they can compose a boundary of any shape by taking arbitrary proportions, even without the participant of coherent twin boundary. This explains the large deviation of a twin boundary from the twinning plane that was often observed in bulk scale samples [15,16]. But what controls the proportion of BP steps still needs further research. In 3D space, the boundary is not linearly inclined away from the twinning plane, but appears as a wavy like terrace. This step nature of the boundary agrees well with the picture of boundary migration dominated by UCR [8,17–19]. During migration, the terrace-like boundary can be divided into many segments. Any segment that is ready for UCR will move a step forward and this finally leads to the observed irregular boundary morphology. Such dynamic behavior suggests that the boundary motion would exhibit a different sensitivity to a precipitate, when compared with twinning dislocation dominated twin boundary migration. For example, if part of the moving boundary encounters a precipitate, other parts can still bypass and finally engulf the precipitate [20–23], instead of being blocked as in the case of a dislocation.

In summary, we have investigated the morphological development in 3D of the boundary produced by UCR. This boundary is significantly different from the well-known twin boundary, which is expected to be parallel to the twinning plane. The mobility of this boundary will be discussed in a separate publication.

The authors declare no competing financial interests.

The authors acknowledge the support provided by grants from Natural Science Foundation of China (50925104, 11132006, 51231005, 51201127 and 51321003), and 973 Program of China (2010CB631003). We also appreciate the support from the 111 Project of China (B06025). J. Wang was supported by Office of Basic Energy Sciences, Project FWP 06SCPE401, under US DOE Contract No. W-7405-ENG-36. B. Y. Liu thanks the support of Gatan China Scholarship. We thank J. C. Wan, L. Lu, G. Yang and C. L. Jia for assistance in TEM experiments.

[1] J. Weertman, J.R. Weertman, Elementary Dislocation Theory, Macmillan, New York, 1964.
[2] J.W. Christian, S. Mahajan, Prog. Mater. Sci. 39 (1995) 1–157.
[3] Y.T. Zhu, X.Z. Liao, X.L. Wu, Prog. Mater. Sci. 57 (2012) 1–62.
[4] M.D. Uchic, D.M. Dimiduk, J.N. Florando, W.D. Nix, Science 305 (2004) 986–989.
[5] Q. Yu, Z.-W. Shan, J. Li, X. Huang, L. Xiao, J. Sun, E. Ma, Nature 463 (2010) 335–338.
[6] M.H. Yoo, Metall. Mater. Trans. A 12 (1981) 409–418.
[7] Q. Yu, J.X. Zhang, Y.Y. Jiang, Philos. Mag. Lett. 91 (2011) 757–765.
[8] B.Y. Liu, J. Wang, B. Li, L. Lu, X.Y. Zhang, Z.W. Shan, J. Li, C.L. Jia, J. Sun, E. Ma, Nat. Commun. 5 (2014) 3297.
[9] B. Li, E. Ma, Phys. Rev. Lett. 103 (2009) 035503.
[10] B. Li, X.Y. Zhang, Scr. Mater. 71 (2014) 45–48.
[11] J. Wang, S.K. Yadav, J.P. Hirth, C.N. Tomé, I.J. Beyerlein, Mater. Res. Lett. 1 (2013) 126–132.
[12] J. Wang, L. Liu, C.N. Tomé, S.X. Mao, S.K. Gong, Mater. Res. Lett. 1 (2013) 81–88.
[13] Q. Sun, X.Y. Zhang, Y. Ren, J. Tu, Q. Liu, Scr. Mater. 90–91 (2014) 41–44.
[14] Z.W. Shan, JOM 64 (2012) 1229–1234.
[15] X.Y. Zhang, B. Li, X.L. Wu, Y.T. Zhu, Q. Ma, Q. Liu, P.T. Wang, M.F. Horstemeyer, Scr. Mater. 67 (2012) 862–865.
[16] P.G. Partridge, E. Roberts, Acta Metall. 12 (1964) 1205.
[17] H. Zong, X. Ding, T. Lookman, J. Li, J. Sun, Acta Mater. 82 (2015) 295–303.
[18] C.D. Barrett, H. El Kadiri, Acta Mater. 63 (2014) 1–15.
[19] B. Xu, L. Capolungo, D. Rodney, Scr. Mater. 68 (2013) 901–904.
[20] M.A. Gharghouri, G.C. Weatherly, J.D. Embury, Philos. Mag. A 78 (1998) 1137–1149.
[21] J.B. Clark, Acta Metall. 13 (1965) 1281–1289.
[22] N. Stanford, M.R. Barnett, Mater. Sci. Eng. A 516 (2009) 226–234.
[23] J.D. Robson, N. Stanford, M.R. Barnett, Acta Mater. 59 (2011) 1945–1956.